THE JOURNAL OF PHYSICAL CHEMISTRY B

pubs.acs.org/JPCB Article

Solid-State Electron Affinity Analysis of Amorphous Fluorinated Polymer Electret

Seonwoo Kim, Anton Melnyk, Denis Andrienko, and Yuji Suzuki*

Cite This: *J. Phys. Chem. B* 2020, 124, 10507−10513 Read Online

ACCESS | Metrics & More | Article Recommendations | Supporting Information

ABSTRACT: In this study, electron trapping phenomena in amorphous polymer electrets were studied using a solid-state electron affinity analysis by means of molecular dynamics simulations parametrized with *ab initio* calculations. Negatively charged amorphous systems of a cyclic transparent optical polymer (CYTOP) with different end groups were reproduced by molecular dynamics simulations parametrized by density functional theory analysis. Quantum mechanical calculations were performed for electron trapping sites to determine the electron affinity of an isolated molecule. The influence of the amorphous system surrounding the trapping site was considered by accounting for electrostatic interactions with surrounding molecules and multipole induction. A series of analyses were carried out to mimic the conformational diversity of the amorphous system. The calculated solid-state electron affinities were found to adopt a Gaussian-type distribution and were in good accordance with the experimental data for surface potential and thermally stimulated discharge spectra, indicating the reliability of the present analysis for predicting the charging performance of amorphous polymer electrets.

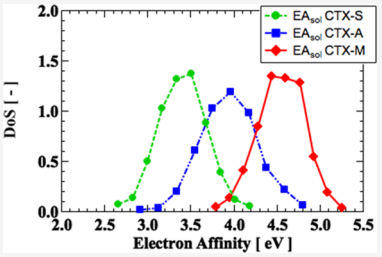

INTRODUCTION

An electret is a dielectric material with quasi-permanent charges. The charges trapped in the material generate an electrostatic field without an external voltage source.[1] Dielectric materials can be charged by various methods including corona ions and soft X-rays.[1−3] In the past few decades, electret-based applications have been developed, with the most broadly used application being electro-acoustic transducers[4−6] such as an electret microphone. Another application is the particle collector[7,8] in which charged electrets attract particles by their electrostatic potential. More recently, electrets have played an important role in vibration-driven energy harvesters (VEHs), which convert ambient kinetic energy into electricity.[9−11] For low vibration frequencies, electret-based VEHs have outstanding potential as power supplies for wireless sensor nodes or wearable devices that can act as a substitutes for traditional batteries.[12−14]

The performance of electret-based devices is strongly dependent on the characteristics of the electret material. First of all, the surface potential of the electret determines the output signal/power of the devices. The transduction efficiency is proportional to the surface potential or surface potential squared. In addition, the long-term stability of trapped charges determines the lifetime of the device.[1,12] Therefore, the development of high-performance electrets is highly desired for realizing practical electret-based devices.

Electret materials can be categorized into two groups: polymer electrets (e.g., polyethylene, polytetrafluoroethylene, Teflon AF, cyclic transparent optical polymer (CYTOP)) and inorganic electrets (e.g., SiO_2). Fluorinated polymer electrets have desirable characteristics: hydrophobicity, chemical/physical stability, and a relatively low process temperature (<300 °C). Some high-performance fluorinated polymers have been proven to stably store trapped charges for more than 20 years.[1,15,16] For Teflon fluorinated ethylene propylene (FEP),[17] a surface potential of about 360 V was obtained for a 12.5 μm-thick sample, corresponding to a surface charge density of 0.54 mC m^{-2}. For Teflon AF[18] and fluorinated polyimide 6FDA/6FDC,[19] surface potentials of 367 (9 μm thick, 0.28 mC m^{-2}) and 450 V (50 μm-thick, 0.27 mC m^{-2}) were reported. Lo and Tai[20] found that parylene-HT can realize a high surface potential of 1380 V (7.3 μm thick, 3.69 mC m^{-2}).

The CYTOP is an amorphous fluorinated polymer with 500−1000 repeat units of five-membered ring structures. It has interesting characteristics distinct from other fluoropolymer electrets, e.g., the charging performance is strongly dependent on the end group, although the number of repeat units is much greater than the number of end groups. There are three types of CYTOPs with different end groups that are commercially available: S-type with trifluoromethyl end groups, A-type with carboxyl end groups, and M-type with amide-alkoxysilane end groups. The surface potentials for 15 μm-thick samples are 250 V (0.25 mC m^{-2}) for S-type, 850 V (0.85 mC m^{-2}) for A-type,

Received: July 16, 2020
Revised: October 7, 2020
Published: November 5, 2020

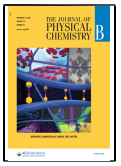

and 1300 V (1.3 mC m^{-2}) for M-type.[21] Sakane et al.[22] improved the charging performance of CYTOP A-type by introducing excessive aminosilane into it (CYTOP EGG). They achieved a very high surface potential of 2000 V with 15 μm-thick films (2.0 mC m^{-2}). Later, Kashiwagi et al.[23] attributed the enhancement of the charging performance to aminosilane-based nanoclusters formed in the film during thermal curing. Recently, a practical rotational electret energy harvester was developed with CYTOP EGG.[24] A 15 μm-thick electret was charged to 850 V, achieving an 80 μW output obtained from an arm swing motion during human walking (height: 1.76 m, weight: 71 kg) at 1.45 m s^{-1}.

Although various fluorinated polymer electrets have been proposed, they were discovered by experiments based on empirical approaches because little quantitative knowledge is available for the charge trapping mechanisms. Based on a band gap model,[25,26] one can assume that many charge traps with different energy depths would exist in dielectric materials. The distribution of such a trap depth forms a density of state, which defines the charge trapping phenomenon for the system. Charges stored in deep traps should remain secure, while those captured in shallow traps can easily be released. However, these previous concepts do not provide any reliable insights for designing new electrets with higher performance.

Since the early 2000s, quantum chemical analysis has been utilized to analyze charge trapping in polymer materials for electrical insulation. Meunier et al.[27,28] investigated polyethylene (PE) by calculating the electron affinity of chemical species in bulk PE. They found that the PE chain itself has negative electron affinity; hence, it is naturally electrophobic. Electrons introduced into the system may easily move to a low volumetric density region or chemical oddity. Therefore, electron traps in PE strongly depend on its morphology or impurities. Wang et al.[29] and Saiz et al.[30] explored the morphologies of PE (e.g., lamellar, crystalline, and amorphous) to study the mobility and location of trapped electrons in PE. Takada et al.[31] analyzed PE, ethylene-tetra-fluoro-ethylene (ETFE), poly-tetra-fluoro-ethylene (PTFE), and polyimide, focusing on their intermolecular structures. They showed that the chemical specificity can cause intermolecular charge localization and create trap sites.

In our previous study, we first adopted quantum chemical analysis to study electron trapping phenomena in amorphous fluorinated polymer electrets.[32] The energy of the orbital where the electron was trapped was selected as the electron affinity based on Koopman's theorem.[33,34] The CYTOP with three different end groups was analyzed. The electron affinity was obtained by long-range corrected density functional theory (DFT) for tetramer molecules with the end groups in vacuum. It was found that electrons trapped in the CYTOP are localized at the end groups, showing that the end group serves as the trap sites. However, it was also found that the simulated electron affinities were considerably overestimated; the electron affinity of CYTOP S-type directly measured by low-energy inverse photoelectron spectroscopy (LEIPS) is 3.6 eV, which is considerably lower than the simulated electron affinity (4.39 eV). This discrepancy seems to stem from the following reasons: (i) in real polymer systems, structural transformation of a molecule is interfered with other surrounding molecules, and thus, the molecule cannot freely relax its geometry to the ground-state structure for a given electronic state. (ii) A molecule naturally has electrostatic potential and interacts with the electrostatic field formed by the neighboring molecules. The energy shift of the molecule due to the electrostatic interaction was neglected in the single-molecule analysis. (iii) Only one tetramer molecule was analyzed for each case, and thus, structural diversity in real systems was not well represented.

In the present study, we aimed to perform a proper evaluation of electron affinity of the CYTOP by the solid-state analysis. Molecular systems of S-type, A-type, and M-type with a molecular weight of approximately 300,000 were generated to mimic the amorphous polymer system. The solid-state electron affinity was obtained by considering electrostatic multipole interaction with surrounding molecules and the electron trapping site. The density of states for electron affinity was computed by considering the morphological diversity of polymeric systems.

THEORETICAL METHOD

The amorphous polymer CYTOP is analyzed by molecular dynamics simulations, quantum mechanical calculations, and multipole analysis. Quantum mechanical calculations are a potent tool for analyzing the electronic states of molecules. However, its computational cost increases exponentially with the number of atoms in the system so that it is too expensive to analyze the whole amorphous system. Instead, because electron trapping sites of CYTOP electrets are mainly localized at end groups,[32] we can split the CYTOP molecule (~1080 repeat units) into a hexamer with an end group for representing the electron trap site and other hexamers distant from the end group, as explained below.

The electron affinity is used to evaluate the electron trap energy in the CYTOP. Among different definitions of molecular electron affinity,[35] we have chosen the vertical electron affinity of detachment, corresponding to the energy necessary for removing a trapped electron, as given in eq 1.

$$\mathrm{EA}_{\mathrm{vd}} = U(g(e), s(n)) - U(g(e), s(e)) \tag{1}$$

Here, $U(g(x), s(x))$ is the energy of the molecule in the electronic state $s(x)$ ($x = n$ for a neutral state, $x = e$ for a negatively charged state) and the equilibrated geometry $g(x)$. The geometry is kept at the negatively charged state because structural relaxation of the electron trap site before/after electron detachment is suppressed by the molecules surrounding the trap site. The subscript vd in $\mathrm{EA}_{\mathrm{vd}}$ will be omitted, and the energy for the equilibrated anionic geometry $U(g(e), s(x))$ will be shortened to $U(x)$ below for simplicity.

The solid-state energy of a trap site is calculated as[36]

$$U_{\mathrm{sol}} = U_{\mathrm{qm}} + U_{\mathrm{elec}} + U_{\mathrm{ind}} \tag{2}$$

where U_{qm} is the quantum mechanical energy of an electron trap site, U_{elec} is the electrostatic energy shift due to the surrounding molecules, and U_{ind} is a compensation term for multipole induction expressed as a second-order energy correction of the Hamiltonian. U_{qm} is computed by DFT calculation with the CAM-B3LYP functional[37−40] and 6-31+G(d,p) basis set using Gaussian09.[41] U_{elec} can be obtained by treating the external field generated by the surrounding molecules as a perturbation term in the molecular Hamiltonian. Using the spherical harmonic addition theorem, the electrostatic interaction between molecules can be expressed by multipole−multipole interactions.[36,42] For U_{ind}, the distributed multipole analysis (DMA) approach[43] is employed to convert the quantum mechanical electron density matrix

https://dx.doi.org/10.1021/acs.jpcb.0c06505
J. Phys. Chem. B 2020, 124, 10507−10513

into the multipole moments. The electron density obtained by DFT calculation is converted to multipoles of rank 0−4 by the GDMA program.[43,44] To make the charge distribution reflect the characteristics of the quantum mechanical wave function, Thole's model[45,46] is adopted with a = 0.39 as the smearing exponent, referring to the AMOEBA force field.[47,48] These two terms are computed by the algorithm built into VOTCA-CTP.[49] When we compute eq 1 using only the quantum mechanical energy of an electron trap site molecule U_{qm}, the single molecular electron affinity (EA_{qm}) is obtained. The solid-state electron affinity (EA_{sol}) is retrieved from the net energy U_{sol}.

Figure 1 displays the chemical structure of the CYTOP series (AGC Co. Ltd.). Each repeat unit has a perfluorinated

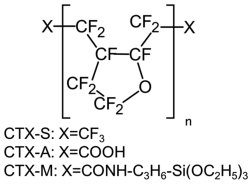

Figure 1. Chemical structure of CYTOP; CTX-S, CTX-A, and CTX-M have different end groups.

pentagonal ring structure. A single CYTOP polymer chain consists of about 540 repeat units (CYTOP CTL) or 1080 repeat units (CYTOP CTX). Two functional groups are attached at both ends: trifluoromethyl groups (S-type), carboxylic groups (A-type), and amide-alkoxysilane groups (M-type). Preliminary DFT calculations are performed to properly model the amorphous polymer electret system. The structure of the polymer and its length are carefully examined. We found that six units (hexamer) can represent the electron trap in the polymer chain within a 2% error with reasonable calculation costs. Thus, the hexamer is employed for further analysis. Details can be found in the Supporting Information. Figure 2 shows the distribution of trapped electrons in CTX-S, CTX-A, and CTX-M hexamer molecules, visualized with GaussView.[50] For CTX-S, the electron is not localized and easily moves to the other repeat unit when the structure is deformed. On the other hand, the electron trapped in CTX-A and CTX-M is localized near the carboxyl and amide groups, respectively.

To construct a CYTOP CTX system, 90 hexamers are used. One out of 90 is the hexamer with the functional group of interest (trifluoromethyl, carboxyl, or amide-alkoxysilane) at one end and a trifluoromethyl group at the other end. This hexamer will be considered as the electron trap site. The other 89 hexamers have trifluoromethyl end groups at both sides. These hexamers represent the CYTOP polymer chain surrounding the electron trap site. With these 90 hexamers, the ratio of the repeat units to the end groups in the system roughly corresponds to that of the real CYTOP CTX system (about 1:540).

With 90 molecules thus prepared, amorphous polymer systems are constructed by molecular dynamics (MD) simulations with GROMACS.[51] Force field parameters are carefully chosen from the optimized potentials for liquid simulations (OPLS) force field.[52,53] Unknown parameters are fitted using the preliminary quantum mechanical analysis. Details of the MD force field preparation are described in the Supporting Information.

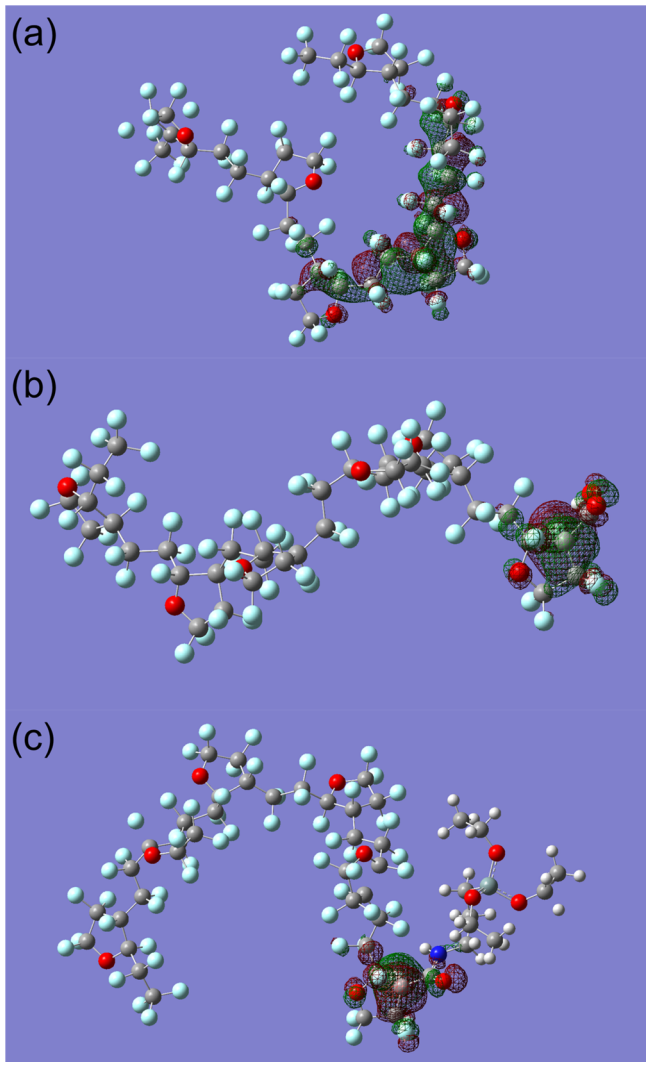

Figure 2. Visualized distribution of the trapped electron in hexamer molecules. (a) CTX-S, (b) CTX-A, and (c) CTX-M. Red and green meshes are positive and negative orbital lobes (gray: carbon, red: oxygen, white: hydrogen, cyan: fluorine, blue: nitrogen).

To achieve an amorphous morphology of the CYTOP in the electrically neutral state, the system is first heated to 800 K with the fixed particle number, volume, and temperature (NVT) condition. The molecules are randomly mixed, and 1000 patterns with identical initial geometries are prepared. Second, the system experiences the annealing process with a constant particle number, pressure, and temperature (NPT). After the temperature was ramped down from 800 to 300 K within 2 ns, the temperature was fixed at 300 K for 1 ns in the NVT condition. The force field parameters for the electron trap site are then updated to the negatively charged one, and an NVT simulation at 300 K is performed for 2 ns. The geometry of the electron trap site transforms to the equilibrium geometry of the anionic state while acknowledging the influence of the surrounding molecules (Figure 3). In total, 1000 negatively charged amorphous CYTOP systems with different initial conditions are computed. The average density of the system is shown in Table 1. The discrepancy between the simulated results and the measurement data (2.03 g cm^{-3}) is less than 5%. It is noted that this difference mainly originates

https://dx.doi.org/10.1021/acs.jpcb.0c06505
J. Phys. Chem. B 2020, 124, 10507−10513

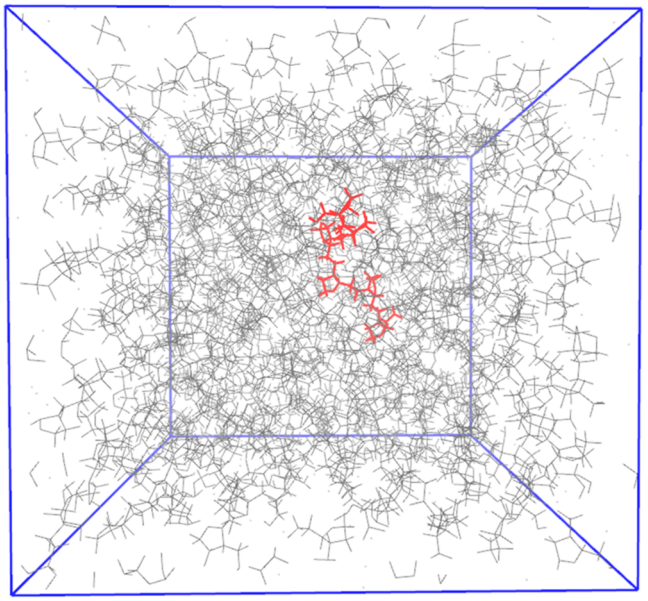

Figure 3. Snapshot of the amorphous morphology of CTX-A generated in the present study. A red molecule is the hexamer with a carboxyl end, representing the part of the polymer chain connected to the end group. Gray hexamers with trifluoromethyl ends embodying repeat units not connected to the end group. The box size is approximately 5.1 nm in each direction. The system is visualized by VMD.[54]

Table 1. Average Density of Generate Amorphous Systems

	CTX-S	CTX-A	CTX-M
ρ_{calc} [g cm^{-3}]	1.95	1.93	1.93

from the shortened chain length; the simulated density slowly increases with the number of repeat units (not shown).

RESULTS AND DISCUSSION

With the geometries obtained, U_{qm}, U_{elec}, and U_{ind} are computed. The single molecular energy U_{qm} calculation is performed for the electron trap site of 1000 systems to obtain the single-molecule electron affinity $EA_{qm} = \{U_{qm}(n) - U_{qm}(e)\}$. The trap site molecule is taken from other molecules and placed in vacuum while maintaining its structure. A single-point DFT calculation is then performed. Figure 4 shows the probability density function for EA_{qm}. The mean values of the Gaussian-like distributions are 4.15 (CTX-M), 3.50 (CTX-A), and 2.99 eV (CTX-S). The order of the mean values (CTX-M > CTX-A > CTX-S) is in qualitative agreement with our previous analysis.[32] The differences of the mean values are more than 0.5 eV, showing significant influence of the end group on the trap energy.

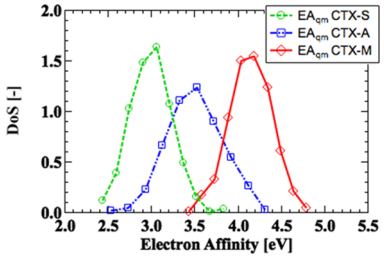

Figure 4. Density of states for the single-molecule electron affinity defined by $EA_{qm} = \{U_{qm}(n) - U_{qm}(e)\}$.

Electrostatic influence on the trap energy is then considered. In Figure 5a, the probability density function for the electrostatic energy shift neglecting multipole induction $EA_{elec} = \{U_{elec}(n) - U_{elec}(e)\}$ is shown. When the multipole induction is neglected, the electron affinity shift for the three different cases shows similar distributions. This is because the electrostatic influence from the surrounding molecules is similar when the backbone molecules are the same. Figure 5b shows the electrostatic energy shift considering the multipole induction $EA_{elec\_ind} = [\{U_{elec}(n) + U_{ind}(n)\} - \{U_{elec}(e) + U_{ind}(e)\}]$. The distributions also have Gaussian-like forms. On the other hand, when both terms are considered, the mean values are shifted as much as 0.6 eV. Also, the distributions become broadened for CTX-S and CTX-A.

Finally, the density of states for solid-state electron affinity defined as $EA_{sol} = \{U_{sol}(n) - U_{sol}(e)\}$ is shown in Figure 6. The order of the mean values in Figure 6 is the same as in Figure 4, but there are shifts in the electron affinity as large as 0.4 eV. Table 2 summarizes the computational results. It is noted that, with the present solid-state analysis, the electron affinity is 3.4 eV for CTX-S, which is in good agreement with our experimental data using an LEIPS (low energy inverse photoemission spectroscopy) value of 3.6 eV[32] within the uncertainties of the simulation results and the experimental data (Table 3).

Figure 7 shows the open-circuit thermally stimulated discharge (TSD) spectra obtained for 15 μm-thick films of CTX-S, CTX-A, and CTX-M. In TSD, the temperature of the electret sample is linearly ramped up, and the leakage current is measured in real time. The sample is charged to a surface potential of about 1 kV by soft X-rays before experiments. The ramp-up speed is 1 °C min^{-1}. When the molecular structure is rigid until discharge, the release of the trapped charge carriers is induced solely by the thermal energy. On the other hand, when the structural relaxation takes place before discharge, the mobile chain segments shake off electrons (wet dog effect) even when the introduced thermal energy is lower than the charge trap energy.[55−57] The wet dog effect can also be explained from the viewpoint of quantum mechanics; the trap energy changes when the geometry is changed. When the temperature becomes higher than the glass transition temperature (T_g), the molecular structure will change, leading to lowering of the electron affinity and then to releasing trapped charges.

Because T_g for the CYTOP (108 °C) is lower than the peak temperature for TSD, the TSD data only give qualitative information on the thermal stability of charges. Still, the peak temperature can be used as the index of thermal stability of trapped charges. It is because the order of the peak position in TSD (CTX-M > CTX-A > CTX-S) is in qualitative agreement with the mean value of electron affinity distributions, as shown in Table 2.

It is noted that photoinduced detrapping measurements (PSD)[56−58] should be a useful tool to measure the charge trap energy of high electron affinity polymers. In PSD, an electret is irradiated with UV photons for discharging the trapped charges while maintaining the polymer temperature. Direct comparison between the present simulation results and the PSD data will be reported elsewhere.

It is emphasized that the electron trap energy can be estimated with the present simulation for solid-state electron

https://dx.doi.org/10.1021/acs.jpcb.0c06505
J. Phys. Chem. B 2020, 124, 10507−10513

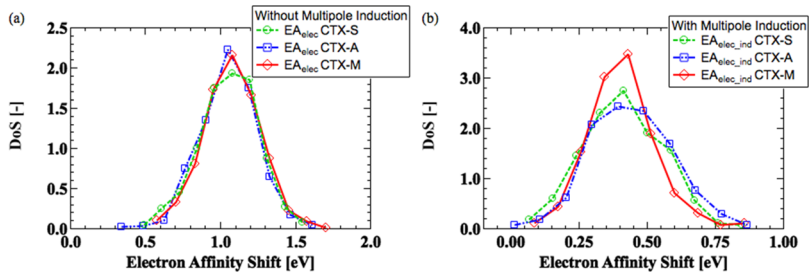

Figure 5. Density of states of the electron affinity shift by the electrostatic interaction from surrounding molecules: (a) $EA_{elec} = \{U_{elec}(n) - U_{elec}(e)\}$ and (b) $EA_{elec\_ind} = [\{U_{elec}(n) + U_{ind}(n)\} - \{U_{elec}(e) + U_{ind}(e)\}]$.

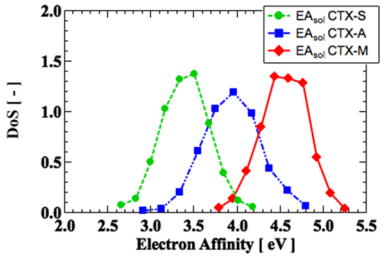

Figure 6. Density of states of the solid-state electron affinity defined by $EA_{sol} = \{U_{sol}(n) - U_{sol}(e)\}$.

Table 2. Distribution Profiles for the Density of State[a]

	CTX-S	CTX-A	CTX-M
μ_{qm}	2.99	3.50	4.15
σ_{qm}	0.342	0.460	0.349
μ_{shift}	0.407	0.432	0.399
σ_{shift}	0.307	0.218	0.221
μ_{sol}	3.40	3.94	4.57
σ_{sol}	0.397	0.465	0.390

[a] μ is the mean value, and σ is the standard deviation (unit: eV).

Table 3. Comparison of the Electron Affinity of CTX-S Obtained from the Energy of the Electron-Trapped Orbital Using Koopman's Theorem,[32] the Present Single Molecular and Solid-State Analysis, and LEIPS Measurement[32]

method	Koopman's theorem[32]	single molecular analysis (present)	solid-state analysis (present)	LEIPS measurement[32]
EA [eV]	4.39	2.99	3.4	3.6 (±0.2)

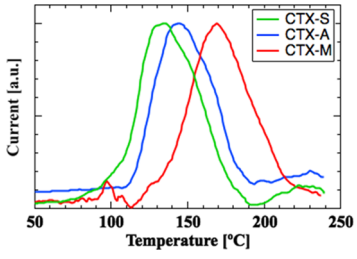

Figure 7. Normalized TSD curves. The peak temperatures are 134 (CTX-S), 144 (CTX-A), and 169 °C (CTX-M). The original curve is taken from Kim et al.[32]

affinity. Without labor-intensive chemical synthesis and charging performance evaluation experiments, we can examine new electret material candidates efficiently and develop a strategy for improving charging performance. Because the computational load for solid-state analysis is high, single-molecule electron affinity analysis is still useful for initial screening of candidates and identifying the charge trap site. After screening, the present solid-state analysis should be performed for more precise evaluation to propose new polymer electret materials.

CONCLUSIONS

In this study, for the first time, we performed solid-state electron affinity analysis of polymer electrets. An amorphous morphology of the CYTOP system is prepared by parameter-fitted molecular dynamics simulations. The quantum mechanical energy for the electron trap site and electrostatic energy shift due to surrounding molecules are considered, while the diversity of molecule conformations is taken into account. The simulated solid-state vertical electron affinity for CTX-S is in good agreement with the electron affinity measured with LEIPS, showing that the present method can properly evaluate electron traps in amorphous polymer electrets. In addition, it is found that the simulated electron affinities for the CYTOP with different end groups are in qualitative agreement with our experimental data using thermally stimulated discharge, indicating the predictive power of the present solid-state analysis for designing a new amorphous polymer electret.

ASSOCIATED CONTENT

Supporting Information

The Supporting Information is available free of charge at https://pubs.acs.org/doi/10.1021/acs.jpcb.0c06505.

Supporting information showing the preliminary quantum chemical analyses for preparing CYTOP CTX systems (PDF)

AUTHOR INFORMATION

Corresponding Author

Yuji Suzuki − *Department of Mechanical Engineering, The University of Tokyo, Bunkyo-ku, Tokyo 113-8656, Japan;* orcid.org/0000-0002-6844-1449; Email: ysuzuki@mesl.t.u-tokyo.ac.jp

Authors

Seonwoo Kim − *Department of Mechanical Engineering, The University of Tokyo, Bunkyo-ku, Tokyo 113-8656, Japan;* orcid.org/0000-0003-4595-5081

Anton Melnyk − *Max Planck Institute for Polymer Research, Mainz 55128, Germany*

Denis Andrienko − *Max Planck Institute for Polymer Research, Mainz 55128, Germany;* orcid.org/0000-0002-1541-1377

Complete contact information is available at:

https://pubs.acs.org/10.1021/acs.jpcb.0c06505

Author Contributions

The manuscript was written through contributions of all authors. All authors have given approval to the final version of the manuscript.

Notes

The authors declare no competing financial interest.

■ ACKNOWLEDGMENTS

This work is partially supported by JST CREST (JPMJCR15Q3 and JPMJCR19Q1). The computational work in this paper is performed by the computer cluster of the Max Planck Institute of Polymer Research and the facilities of the ISSP Supercomputer Center, the University of Tokyo. S.K. is supported through the Leading Graduate Schools Program, "Global Leader Program for Social Design and Management", by MEXT Japan.

■ REFERENCES

(1) Sessler, G. M. *Electrets*; 3rd Edition; Laplacian Press: 1998.
(2) Giacometti, J. A.; Oliveira, O. N. Corona Charging of Polymers. *IEEE Trans. Electr. Insul.* **1992**, *27*, 924−943.
(3) Hagiwara, K.; Goto, M.; Iguchi, Y.; Tajima, T.; Yasuno, Y.; Kodama, H.; Kidokoro, K.; Suzuki, Y. Electret Charging Method Based on Soft X-Ray Photoionization for MEMS Transducers. *IEEE Trans. Dielectr. Electr. Insul.* **2012**, *19*, 1291−1298.
(4) Sessler, G. M.; West, J. E. Electret Transducers: A Review. *J. Acoust. Soc. Am.* **1973**, *53*, 1589−1600.
(5) Heydt, R.; Pelrine, R.; Joseph, J.; Eckerle, J.; Kornbluh, R. Acoustical Performance of an Electrostrictive Polymer Film Loudspeaker. *J. Acoust. Soc. Am.* **2000**, *107*, 833−839.
(6) Bai, M. R.; Wang, C.-J.; Chiang, D.-M.; Lin, S.-R. Experimental Modeling and Design Optimization of Push-pull Electret Loudspeakers. *J. Acoust. Soc. Am.* **2010**, *127*, 2274−2281.
(7) Van Turnhout, J.; Adamse, J. W. C.; Hoeneveld, W. J. Electret Filters for High-Efficiency Air Cleaning. *J. Electrostat.* **1980**, *8*, 369−379.
(8) Li, Y.; Yin, X.; Si, Y.; Yu, J.; Ding, B. All-Polymer Hybrid Electret Fibers for High-Efficiency and Low-Resistance Filter Media. *Chem. Eng. J.* **2020**, *398*, 125626.
(9) Roundy, S.; Wright, P. K.; Rabaey, J. A Study of Low Level Vibrations as a Power Source for Wireless Sensor Nodes. *Comput. Commun.* **2003**, *26*, 1131−1144.
(10) Mitcheson, P. D.; Green, T. C.; Yeatman, E. M.; Holmes, A. S. Architectures for Vibration-Driven Micropower Generators. *J. Microelectromech. Syst.* **2004**, *13*, 429−440.
(11) Beeby, S. P.; Tudor, M. J.; White, N. M. Energy Harvesting Vibration Sources for Microsystems Applications. *Meas. Sci. Technol.* **2006**, *17*, R175.
(12) Suzuki, Y. Recent Progress in MEMS Electret Generator for Energy Harvesting. *IEEJ Trans. Electr. Electron. Eng.* **2011**, *6*, 101−111.
(13) Boisseau, S.; Despesse, G.; Ricart, T.; Defay, E.; Sylvestre, A. Cantilever-Based Electret Energy Harvesters. *Smart Mater. Struct.* **2011**, *20*, 105013.
(14) Honma, H.; Mitsuya, H.; Hashiguchi, G.; Fujita, H.; Toshiyoshi, H. Improvement of Energy Conversion Effectiveness and Maximum Output Power of Electrostatic Induction-type MEMS Energy Harvesters by Using Symmetric Comb-electrode Structures. *J. Micromech. Microeng.* **2018**, *28*, No. 064005.
(15) Kotrappa, P. Long Term Stability of Electrets Used in Electret Ion Chambers. *J. Electrostat.* **2008**, *66*, 407−409.
(16) Mekishev, G. A.; Yovcheva, T. A.; Gentcheva, E. A.; Nedev, S. R. Study of Electrets Stored at Pressures Lower than Atmospheric. *J. Electrostat.* **2005**, *63*, 1009−1015.
(17) Tada, Y. Experimental Characteristics of Electret Generator Using Polymer Film Electrets. *Jpn. J. Appl. Phys.* **1992**, *31*, 846−851.
(18) Boland, J.; Chao, Y.-H.; Suzuki, Y.; Tai, Y. C. Micro Electret Power Generator. In *16th IEEE International Conference on Micro Electro Mechanical Systems (MEMS'03)*; IEEE: Kyoto, Japan, 2003; pp. 538−541.
(19) Erhard, D. P.; Richter, F.; Bartz, C. B. A.; Schmidt, H. W. Fluorinated Aromatic Polyimides as High-Performance Electret Materials. *Macromol. Rapid Commun.* **2015**, *36*, 520−527.
(20) Lo, H. W.; Tai, Y. C. Parylene-Based Electret Power Generators. *J. Micromech. Microeng.* **2008**, *18*, 104006.
(21) Tsutsumino, T.; Suzuki, Y.; Kasagi, N.; Sakane, Y. Seismic Power Generator Using High-Performance Polymer Electret. In *19th IEEE International Conference on Micro Electro Mechanical Systems (MEMS'06)*; IEEE: Istanbul, Turkey, 2006; pp. 98−101.
(22) Sakane, Y.; Suzuki, Y.; Kasagi, N. The Development of a High-Performance Perfluorinated Polymer Electret and Its Application to Micro Power Generation. *J. Micromech. Microeng.* **2008**, *18*, 104011.
(23) Kashiwagi, K.; Okano, K.; Miyajima, T.; Sera, Y.; Tanabe, N.; Morizawa, Y.; Suzuki, Y. Nano-Cluster-Enhanced High-Performance Perfluoro-Polymer Electrets for Energy Harvesting. *J. Micromech. Microeng.* **2011**, *21*, 125016.
(24) Miyoshi, T.; Adachi, M.; Suzuki, K.; Liu, Y.; Suzuki, Y. Low-Profile Rotational Electret Generator Using Print Circuit Board for Energy Harvesting from Arm Swing. In *The 31st IEEE International Conference on Micro Electro Mechanical Systems (MEMS 2018)*; IEEE: Belfast, Northern Ireland, 2018; pp. 230−232.
(25) Yilmaz, F. *Conducting Polymers*; IntechOpen: 1997, Vol. 2.
(26) Kaake, L. G.; Barbara, P. F.; Zhu, X. Y. Intrinsic Charge Trapping in Organic and Polymeric Semiconductors: A Physical Chemistry Perspective. *J. Phys. Chem. Lett.* **2010**, *1*, 628−635.
(27) Meunier, M.; Quirke, N. Molecular Modeling of Electron Trapping in Polymer Insulators. *J. Chem. Phys.* **2000**, *113*, 369.
(28) Meunier, M.; Quirke, N.; Aslanides, A. Molecular Modeling of Electron Traps in Polymer Insulators: Chemical Defects and Impurities. *J. Chem. Phys.* **2001**, *115*, 2876−2881.
(29) Wang, Y.; MacKernan, D.; Cubero, D.; Coker, D. F.; Quirke, N. Single Electron States in Polyethylene. *J. Chem. Phys.* **2014**, *140*, 154902.
(30) Saiz, F.; Cubero, D.; Quirke, N. The Excess Electron at Polyethylene Interfaces. *Phys. Chem. Chem. Phys.* **2018**, *20*, 25186−25194.
(31) Takada, T.; Kikuchi, H.; Miyake, H.; Tanaka, Y.; Yoshida, M.; Hayase, Y. Determination of Charge-Trapping Sites in Saturated and Aromatic Polymers by Quantum Chemical Calculation. *IEEE Trans. Dielectr. Electr. Insul.* **2015**, *22*, 1240−1249.
(32) Kim, S.; Suzuki, K.; Sugie, A.; Yoshida, H.; Yoshida, M.; Suzuki, Y. Effect of End Group of Amorphous Perfluoro-Polymer Electrets on Electron Trapping. *Sci. Technol. Adv. Mater.* **2018**, *19*, 486−494.
(33) Koopmans, T. Über Die Zuordnung von Wellenfunktionen Und Eigenwerten Zu Den Einzelnen Elektronen Eines Atoms. *Physica* **1934**, *1*, 104−113.
(34) Tsuneda, T.; Song, J. W.; Suzuki, S.; Hirao, K. On Koopmans' Theorem in Density Functional Theory. *J. Chem. Phys.* **2010**, *133*, 174101.
(35) Rienstra-Kiracofe, J. C.; Tschumper, G. S.; Schaefer, H. F.; Nandi, S.; Ellison, G. B. Atomic and Molecular Electron Affinities: Photoelectron Experiments and Theoretical Computations. *Chem. Rev.* **2002**, *102*, 231−282.
(36) Andrienko, D. Simulations of Morphology and Charge Transport in Supramolecular Organic Materials. *Supramol. Mater. Opto-Electron.* **2014**, *12*, 309.
(37) Becke, A. D. A New Mixing of Hartree-Fock and Local Density-Functional Theories. *J. Chem. Phys.* **1993**, *98*, 1372−1377.
(38) Lee, C.; Yang, W.; Parr, R. G. Development of the Colle-Salvetti Correlation-Energy Formula into a Functional of the Electron Density. *Phys. Rev. B* **1988**, *37*, 785−789.

(39) Vosko, S. H.; Wilk, L.; Nusair, M. Accurate Spin-Dependent Electron Liquid Correlation Energies for Local Spin Density Calculations: A Critical Analysis. *Can. J. Phys.* **1980**, *58*, 1200−1211.
(40) Yanai, T.; Tew, D. P.; Handy, N. C. A New Hybrid Exchange-Correlation Functional Using the Coulomb-Attenuating Method (CAM-B3LYP). *Chem. Phys. Lett.* **2004**, *393*, 51−57.
(41) Frisch, M.; Trucks, G. W.; Schlegel, H. B.; Scuseria, G. E.; Robb, M. A.; Cheeseman, J. R.; Scalmani, G.; Barone, V.; Mennucci, B.; Petersson, G.; et al. *Gaussian 09*; Revision a. 02, Gaussian. Gaussian, Inc.: Wellingford, CT, 2009.
(42) Stone, A. J. *The Theory of Intermolecular Forces*; Oxford University Press: 2013, DOI: 10.1093/acprof:oso/9780199672394.001.0001.
(43) Stone, A. J.; Alderton, M. Distributed Multipole Analysis: Methods and Applications. *Mol. Phys.* **1985**, *56*, 1047−1064.
(44) Stone, A. J. Distributed Multipole Analysis: Stability for Large Basis Sets. *J. Chem. Theory Comput.* **2005**, *1*, 1128−1132.
(45) Thole, B. T. Molecular Polarizabilities Calculated with a Modified Dipole Interaction. *Chem. Phys.* **1981**, *59*, 341−350.
(46) Van Duijnen, P. T.; Swart, M. Molecular and Atomic Polarizabilities: Thole's Model Revisited. *J. Phys. Chem. A* **1998**, *102*, 2399−2407.
(47) Ren, P.; Ponder, J. W. Polarizable Atomic Multipole Water Model for Molecular Mechanics Simulation. *J. Phys. Chem. B* **2003**, *107*, 5933−5947.
(48) Ponder, J. W.; Wu, C.; Ren, P.; Pande, V. S.; Chodera, J. D.; Schnieders, M. J.; Haque, I.; Mobley, D. L.; Lambrecht, D. S.; DiStasio, R. A., Jr.; Head-Gordon, M. Current Status of the AMOEBA Polarizable Force Field. *J. Phys. Chem. B* **2010**, *114*, 2549−2564.
(49) Rühle, V.; Lukyanov, A.; May, F.; Schrader, M.; Vehoff, T.; Kirkpatrick, J.; Baumeier, B.; Andrienko, D. Microscopic Simulations of Charge Transport in Disordered Organic Semiconductors. *J. Chem. Theory Comput.* **2011**, *7*, 3335−3345.
(50) Dennington, R.; Keith, T.; Millam, J.; et al. *GaussView*; Version 5. Gaussian, Inc.: 2009.
(51) Pronk, S.; Páll, S.; Schulz, R.; Larsson, P.; Bjelkmar, P.; Apostolov, R.; Shirts, M. R.; Smith, J. C.; Kasson, P. M.; Van Der Spoel, D.; et al. GROMACS 4.5: A High-Throughput and Highly Parallel Open Source Molecular Simulation Toolkit. *Bioinformatics* **2013**, *29*, 845−854.
(52) Jorgensen, W. L.; Tirado-Rives, J. The OPLS Potential Functions for Proteins. Energy Minimizations for Crystals of Cyclic Peptides and Crambin. *J. Am. Chem. Soc.* **1988**, *110*, 1657−1666.
(53) Kaminski, G. A.; Friesner, R. A.; Tirado-Rives, J.; Jorgensen, W. L. Evaluation and Reparametrization of the OPLS-AA Force Field for Proteins via Comparison with Accurate Quantum Chemical Calculations on Peptides. *J. Phys. Chem. B* **2001**, *105*, 6474−6487.
(54) Humphrey, W.; Dalke, A.; Schulten, K. VMD: Visual Molecular Dynamics. *J. Mol. Graphics* **1996**, *14*, 33−38.
(55) Kryszewski, M.; Ulański, J.; Jeszka, J. K.; Zieliński, M. Chain and Carrier Mobility in Polymer Systems as Investigated by Thermally Stimulated Current Techniques. *Polym. Bull.* **1982**, *8*, 187−192.
(56) Mellinger, A.; Camacho González, F.; Gerhard-Multhaupt, R. Ultraviolet-Induced Discharge Currents and Reduction of the Piezoelectric Coefficient in Cellular Polypropylene Films. *Appl. Phys. Lett.* **2003**, *82*, 254−256.
(57) Mellinger, A.; González, F. C.; Gerhard-Multhaupt, R. Photostimulated Discharge in Electret Polymers: An Alternative Approach for Investigating Deep Traps. *IEEE Trans. Dielectr. Electr. Insul.* **2004**, *11*, 218−226.
(58) Oda, T.; Utsumi, T.; Kumano, T.; Itami, M. Observation of Photo-Stimulated Detrapping Currents of FEP Teflon Electrets. In *1985 5th International Symposium on Electrets (ISE 5)*; IEEE: 1985; pp. 288−293.

https://dx.doi.org/10.1021/acs.jpcb.0c06505
J. Phys. Chem. B 2020, 124, 10507−10513